A Viscoelastic Model for the Rate Effect in Transfer Printing

H. Cheng[1,†], M. Li[2,†], J. Wu[3,4,*], A. Carlson[5], S. Kim[6], Y. Huang[1], Z. Kang[2], K.-C. Hwang[3,4], and J.A. Rogers[5,*]

[1] *Department of Mechanical Engineering and Department of Civil and Environmental Engineering, Northwestern University, Evanston, IL 60208, USA*

[2] *State Key Laboratory of Structural Analysis for Industrial Equipment, Dalian University of Technology, Dalian 116024, China*

[3]*AML, Department of Engineering Mechanics, Tsinghua University, Beijing 100084, China*

[4]*Center for Mechanics and Materials, Tsinghua University, Beijing 100084, China*

[5]*Department of Materials Science and Engineering; Materials Research Laboratory; and Beckman Institute, University of Illinois, Urbana, Il 61801, USA*

[6]*Department of Mechanical Science and Engineering, University of Illinois, Urbana, IL 61801, USA*

Abstract: Transfer printing is a volatile tool to retract micro devices from a donor substrate via elastomeric stamps, from which the devices are grown or fabricated, followed by printing to a receiver substrate where the device is assembled to an array for integration in various applications. Among five approaches of transfer printing summarized in the paper, the viscoelastic property of stamps is widely adopted to modulate the interfacial adhesion between the stamp and devices by applying different pulling speed. A viscoelastic model for transfer printing is established analytically. It shows that the interfacial adhesion increases with pulling speed, which is verified by the experiments and numerical simulations.

---

† – H.C., M.L. contributed equally to this work.

* – To whom correspondence may be addressed. Email: wujian@tsinghua.edu.cn and jrogers@illinois.edu

Keywords: *transfer printing, viscoelasticity, interfacial fracture toughness, pulling speed, pull-off force.*

1. Introduction

Transfer printing has evolved into an exceptionally sophisticated approach to materials assembly and micro-/nanofabrication. It retracts (picks up) "inks", here defined as a diversity of material classes with a wide range of geometries and configurations, from their growth (donor) substrate via an elastomeric stamp, and then prints them onto a different (receiver) substrate [1-18]. Recent rapid progress in the field has significantly expanded the range of materials for patterning and their applications.

There are several approaches in transfer printing to retract the inks from the donor substrate and to print them onto the receiver substrate.

(1) Kinetically-controlled transfer printing [1, 2]. The inks are retracted rapidly by an elastomeric stamp, and printed slowly to make use of the high and low adhesion strengths respectively at large and small peeling rates due to viscoelasticity of the stamp.

(2) Surface-relief-assisted transfer printing [3-6]. The inks are retracted by an elastomeric stamp with the surface relief structures, such as microtips, to achieve large surface contact with the inks (and therefore large adhesion force) during retraction, and small contact area during printing.

(3) Load-enhanced transfer printing [9, 19-23]. Different mechanical loading protocols are adopted to facilitate large and small adhesion forces during retraction and printing, respectively, such as shear-enhanced transfer printing [7, 8] that which mechanically initiates separation at the adhesive surface via directional shearing at the interface to control the printing of inks.

(4) Laser-driven transfer printing [15, 16]. During printing a laser pulse initiates separation at the adhesive surface due to large thermal mismatch between the stamp and inks.

(5) Active-pressure-control-assisted transfer printing. [24]. Surface adhesion can be modulated by pressurizing microchannels under a thin layer of membrane in a controlled manner to induce a

variety level of surface deformation via inflation in printing.

The viscoelastic property [25, 26] of elastomeric stamps is one of the most important and frequently used properties to modulate the range of "printable" materials based on the pioneering work of Schapery [27, 28] and Gent et al. [29]. The adhesion of the elastomeric stamp increases with the pulling speed [30, 31], and the rate dependence has also been studied by Rahulkumar et al. [32]. Rapid acquisition (pickup) of inks allows for high adhesion to the stamp. This process is followed by a slow retraction to successfully print them onto the receiver substrates [1, 2].

Figure 1a represents a schematic illustration for transfer printing with an elastomeric stamp comprising of a single, rectangular post mounted on a thick backing layer [4, 7, 8]. Posts were brought into direct contact with the underlying inks of the same lateral dimension in the experiments. The poly(dimethylsiloxane) (PDMS, 5:1 monomer:catalyst mix ratio) stamp ($0.1\times0.1\times0.1mm$) formed conformal contact with the ink ($0.1\times0.1\times0.01mm$) during retraction and printing. The pull-off force F in the normal direction, required to remove PDMS posts from fixed silicon inks, was measured using a custom setup to evaluate the adhesion under different pulling speeds [4].

This paper aims at studying the effect of pulling speed on transfer printing. A viscoelastic model for the delamination of stamp/ink interface is established in Section 2, which provides an analytical relation between the pull-off force F and pulling speed v of the stamp. The results are compared with the experiments and numerical results obtained by the finite element method in Section 3. The combined analytical/experimental/numerical studies provide not only the fundamental understanding of rate-dependent transfer printing but also useful design guidelines for transfer printing.

2. A Viscoelastic Model for Transfer Printing

The relaxation modulus of PDMS in the time domain $E(t)$, normalized by the initial

modulus E_0, can be expressed via the Prony series by $E(t)/E_0 = 1-\sum_{i=1}^{N} g_i\left(1-e^{-t/\tau_i}\right)$, where g_i and τ_i are material parameters. The elastic Young's modulus E_∞ is the limit of $E(t)$ for $t\to\infty$, and is related to E_0 and g_i by $E_\infty = E_0\left(1-\sum_{i=1}^{N} g_i\right)$. The relaxation modulus of PDMS is then expressed as

$$E(t) = E_\infty \frac{1-\sum_{i=1}^{N} g_i\left(1-e^{-t/\tau_i}\right)}{1-\sum_{i=1}^{N} g_i}. \tag{1}$$

The Laplace transform [33] gives the frequency dependence of above relaxation modulus

$$E(\omega) = E_\infty \frac{1-\sum_{i=1}^{N} \frac{g_i}{1+\tau_i^2\omega^2} + j\sum_{i=1}^{N} \frac{g_i\tau_i\omega}{1+\tau_i^2\omega^2}}{1-\sum_{i=1}^{N} g_i}, \tag{2}$$

where $j=\sqrt{-1}$, and the real and imaginary parts of Eq. (2) are called the storage and loss moduli, respectively. Figure 2 shows the storage modulus of PDMS versus the frequency ω in Eq. (2) for the second-order Prony series (N=2) with Young's modulus $E_\infty = 1.32$ MPa, g_1=0.102, g_2=0.209, τ_1=0.426 s and τ_2=0.0167 s, which agrees well with the experimentally measured storage modulus of PDMS (error < 6%). The relaxation modulus is several orders of magnitude smaller than that of the ink (e.g., 130 GPa for silicon).

The pull off of the stamp is characterized by delamination of the post/ink interface, which initiates from the edge of the interface, and is modeled by a small interfacial crack of length *a* at the edge. For the remotely applied stress σ normal to the interface, the interfacial crack tip energy release rate is given by [28]

$$G = \frac{1}{2}\int_0^t C_v(t-\tau)\frac{dK_I^2(\tau)}{d\tau}d\tau, \tag{3}$$

where $C_v(t)$ is a plane-strain creep compliance and its Laplace transform (with respect to time)

$\bar{C}_v$ is related to that of the relaxation modulus $\bar{E} = \int_0^\infty e^{-st} E(t)\,dt$ by $s\bar{C}_v = 3/(4s\bar{E})$ for an incompressible solid [27]; $K_I \approx 1.122\sigma\sqrt{\pi a}$ is the stress intensity factor for an edge crack in a homogeneous solid [34]; and the factor $1/2$ on the right hand side of Eq. (3) accounts for the large elastic mismatch between an incompressible elastic solid (e.g., PDMS with the Poissons' ratio $\nu \approx 0.5$) and a rigid (e.g., silicon) substrate [35]. For a constant remotely applied stress rate $\dot{\sigma}$ (and therefore $\sigma = \dot{\sigma} t$), $K_I \approx 1.122\dot{\sigma} t\sqrt{\pi a}$ such that $K_I^2 \approx 4(\dot{\sigma} t)^2 a$. Equation (3) becomes

$$G = 4\dot{\sigma}^2 a \int_0^t (t-\tau) C_v(\tau)\,d\tau . \tag{4}$$

The crack propagates once the crack tip energy release rate G reaches the interfacial toughness Γ_0, which, together with Eq. (4), gives the following equation to determine the critical time t_c for crack propagation,

$$\int_0^{t_c} (t_c-\tau) C_v(\tau)\,d\tau = \frac{\Gamma_0}{4\dot{\sigma}^2 a}, \tag{5}$$

or equivalently,

$$\dot{\sigma} = \sqrt{\frac{\Gamma_0}{4a}} \left[\int_0^{t_c} (t_c-\tau) C_v(\tau)\,d\tau\right]^{\frac{-1}{2}}. \tag{6}$$

The pull-off force is $F = L^2\dot{\sigma} t_c$, which is given in terms of t_c via Eq. (6) as

$$F = F(t_c) = L^2 \sqrt{\frac{\Gamma_0}{4a}}\, t_c \left[\int_0^{t_c} (t_c-\tau) C_v(\tau)\,d\tau\right]^{\frac{-1}{2}}. \tag{7}$$

The applied strain rate is $\dot{\varepsilon}(t) = C_v(t)\dot{\sigma}$, which gives the pulling speed of the stamp as $v = (h+H)\dot{\varepsilon}(t_c) = (h+H) C_v(t_c)\dot{\sigma}$, where h+H is the total height of the stamp [= sum of the post (h) and backing layer (H) heights, see Fig. 1]. The pulling speed is then obtained in terms of t_c via Eq. (6) as

$$v = v(t_c) = (h+H) \sqrt{\frac{\Gamma_0}{4a}}\, C_v(t_c) \left[\int_0^{t_c} (t_c-\tau) C_v(\tau)\,d\tau\right]^{\frac{-1}{2}}. \tag{8}$$

Equations (7) and (8) are the analytical parametric equations for the pull-off force F and pulling speed v, which give the implicit relation $F=F(v)$.

3. Comparison with Experiments and Numerical Simulations

For the relaxation modulus $E(t)$ of PDMS given in Eq. (1) with the second-order Prony series (N=2) (Fig. 2), the plane-strain creep compliance is given by

$$C_v(t)=\frac{3}{4E_\infty}\left[1+\frac{b_2(\tau_1 b_1-1)(\tau_2 b_1-1)e^{-b_1 t}-b_1(\tau_1 b_2-1)(\tau_2 b_2-1)e^{-b_2 t}}{b_1-b_2}\right], \tag{9}$$

where b_1 and b_2 are the two roots of the quadratic equation $\tau_1\tau_2 x^2-\left[(1-g_2)\tau_1+(1-g_1)\tau_2\right]x+1-g_1-g_2=0$. The energy release rate in Eq. (4) becomes

$$G=\frac{3\dot{\sigma}^2 a}{2E_\infty}\left\{\begin{array}{l}\dfrac{2\tau_1^2\tau_2^2}{(1-g_1-g_2)^2}\dfrac{b_2^3(\tau_1 b_1-1)(\tau_2 b_1-1)e^{-b_1 t}-b_1^3(\tau_1 b_2-1)(\tau_2 b_2-1)e^{-b_2 t}}{b_1-b_2}\\ +\left(t-\dfrac{\tau_1 g_1+\tau_2 g_2}{1-g_1-g_2}\right)^2+2\dfrac{\tau_1^2 g_1+\tau_2^2 g_2}{1-g_1-g_2}+\left(\dfrac{\tau_1 g_1+\tau_2 g_2}{1-g_1-g_2}\right)^2\end{array}\right\}. \tag{10}$$

Finite element method (FEM) is used to validate the above expression of the energy release rate for the crack length a = 2.5 μm, post width L = 100 μm, and applied stress rate $\dot{\sigma}=5.86\times10^5$ Pa/s, where the ink is modeled as a rigid substrate. The plane-strain element CPE8R in the ABAQUS finite element program [36] is used, with very fine mesh (the element length ~ a/1000) around the crack tip. The crack tip energy release rate (as a function of time) is obtained from the contour integral. Several contours are placed around the crack and dissipation zone to ensure the contour integrals are path-independent. Mesh refinement ensures the convergence of numerical results. Figure 3 shows a good agreement between the analytical and numerical results for the same relaxation modulus in Eq. (1).

For the second-order Prony series, Eq. (5) for the critical time becomes

$$\frac{2\tau_1^2\tau_2^2}{\left(1-g_1-g_2\right)^2}\frac{b_2^3\left(\tau_1 b_1-1\right)\left(\tau_2 b_1-1\right)e^{-b_1 t_c}-b_1^3\left(\tau_1 b_2-1\right)\left(\tau_2 b_2-1\right)e^{-b_2 t_c}}{b_1-b_2}$$
$$+\left(t_c-\frac{\tau_1 g_1+\tau_2 g_2}{1-g_1-g_2}\right)^2+2\frac{\tau_1^2 g_1+\tau_2^2 g_2}{1-g_1-g_2}+\left(\frac{\tau_1 g_1+\tau_2 g_2}{1-g_1-g_2}\right)^2-\frac{2E_\infty \Gamma_0}{3\dot{\sigma}^2 a}=0 \quad , \tag{11}$$

which gives the critical time, normalized by τ_1, to depend on non-dimensional parameters in the second-order Prony series g_1, g_2 and τ_2/τ_1, and a combination of applied stress rate, crack length, Young's modulus and interfacial toughness $\left(\dot{\sigma}\tau_1\right)^2 a/\left(E_\infty \Gamma_0\right)$. For g_1=0.102, g_2=0.209 and $\tau_2/\tau_1=.0392$, Figure 4 shows that the normalized critical time t_c/τ_1 decreases with $\left(\dot{\sigma}\tau_1\right)^2 a/\left(E_\infty \Gamma_0\right)$.

Equation (11) can be rewritten to give $\dot{\sigma}$ in terms of t_c as

$$\dot{\sigma}\left(t_c\right)=\sqrt{\frac{E_\infty \Gamma_0}{a}}\left[\begin{array}{l}\dfrac{3\tau_1^2\tau_2^2}{\left(1-g_1-g_2\right)^2}\dfrac{b_2^3\left(\tau_1 b_1-1\right)\left(\tau_2 b_1-1\right)e^{-b_1 t_c}-b_1^3\left(\tau_1 b_2-1\right)\left(\tau_2 b_2-1\right)e^{-b_2 t_c}}{b_1-b_2} \\ +\dfrac{3}{2}\left(t_c-\dfrac{\tau_1 g_1+\tau_2 g_2}{1-g_1-g_2}\right)^2+3\dfrac{\tau_1^2 g_1+\tau_2^2 g_2}{1-g_1-g_2}+\dfrac{3}{2}\left(\dfrac{\tau_1 g_1+\tau_2 g_2}{1-g_1-g_2}\right)^2\end{array}\right]^{\frac{-1}{2}} . \tag{12}$$

Therefore the pull-off force and pulling speed become functions of t_c as $F=L^2 t_c \dot{\sigma}\left(t_c\right)$ and $v=\left(h+H\right)C_v\left(t_c\right)\dot{\sigma}\left(t_c\right)$.

Figure 5 shows the pull-off force F versus the pulling speed v for the second-order Prony series. The numerical results given by FEM and experimental results are also shown. The relaxation modulus is given in Eq. (1); the total height of the stamp is $h+H$ = 1100 μm and post width is L = 100 μm, as in the experiments; the interfacial toughness is $\Gamma_0=0.036$ J/m^2 [37]; and the crack length is a = 2.5 μm. The analytic model shows a good agreement with FEM and experimental data, particularly for the pulling speed greater than 50 μm/s. Numerical results obtained by FEM agree with the experiments for the entire range of pulling speed.

4. Concluding Remarks and Discussions

The analytic model shows an important scaling law that the pull-off force *F*, normalized by $E_\infty L^2$, depends on the interfacial toughness, crack length and Young's modulus via a single, dimensionless combination $\Gamma_0/(aE_\infty)$. The normalized pull-off force also depends on the viscoelastic parameters in the (second-order) Prony series. The analytic model shows that the pull-off force increases as the pulling speed, and agrees well with the experiments and numerical simulations for relatively large pulling speed (>50 μm/s). The analytic model provides important understanding of, and useful design tool for, the rate-dependent transfer printing.

The discrepancy between the analytic model and experiments at small pulling speed may result from the interfacial fracture toughness Γ_0, which decreases with the crack tip speed (therefore the pulling speed *v*) [2]. As Γ_0 decreases at low pulling speed, the scaling law established in the analytical model indicates that the pull-off force would be smaller than that given in Eq. (7) for a constant Γ_0, thereby decreasing the discrepancy between the analytic model and experiments.

Acknowledgments:

Y.H. and J.A.R. acknowledge the support from NSF (OISE-1043143, ECCS-0824129, and CMMI-0749028). K.C.H. and Y.H. also acknowledge the support from NSFC.

References

[1] Meitl, M. A., Zhu, Z. T., Kumar, V., Lee, K. J., Feng, X., Huang, Y. Y., Adesida, I., Nuzzo, R. G., and Rogers, J. A., 2006, "Transfer Printing by Kinetic Control of Adhesion to an Elastomeric Stamp," Nature Materials, 5(1), pp. 33-38.

[2] Feng, X., Meitl, M. A., Bowen, A. M., Huang, Y., Nuzzo, R. G., and Rogers, J. A., 2007, "Competing Fracture in Kinetically Controlled Transfer Printing," Langmuir, 23(pp. 12555-12560.

[3] Kim, S., Carlson, A., Cheng, H., Lee, S., Park, J.-K., Huang, Y., and Rogers, J. A., 2012, "Enhanced Adhesion with Pedestal-Shaped Elastomeric Stamps for Transfer Printing," Applied Physics Letters, 100(17), pp. 171909.

[4] Kim, S., Wu, J. A., Carlson, A., Jin, S. H., Kovalsky, A., Glass, P., Liu, Z. J., Ahmed, N., Elgan, S. L., Chen, W. Q., Ferreira, P. M., Sitti, M., Huang, Y. G., and Rogers, J. A., 2010, "Microstructured Elastomeric Surfaces with Reversible Adhesion and Examples of Their Use in Deterministic Assembly by Transfer Printing," Proceedings of the National Academy of Sciences of the United States of America, 107(40), pp. 17095-17100.

[5] Yang, S. Y., Carlson, A., Cheng, H., Yu, Q., Ahmed, N., Wu, J., Kim, S., Sitti, M., Ferreira, P. M., Huang, Y., and Rogers, J. A., 2012, "Elastomer Surfaces with Directionally Dependent Adhesion Strength and Their Use in Transfer Printing with Continuous Roll-to-Roll Applications," Advanced Materials, 24(16), pp. 2117-2222.

[6] Wu, J., Kim, S., Chen, W., Carlson, A., Hwang, K.-C., Huang, Y., and Rogers, J. A., 2011, "Mechanics of Reversible Adhesion," Soft Matter, 7(18), pp. 8657-8662.

[7] Carlson, A., Kim-Lee, H.-J., Wu, J., Elvikis, P., Cheng, H., Kovalsky, A., Elgan, S., Yu, Q., Ferreira, P. M., Huang, Y., Turner, K. T., and Rogers, J. A., 2011, "Shear-Enhanced Adhesiveless Transfer Printing for Use in Deterministic Materials Assembly," Applied Physics Letters, 98(26), pp. 264104.

[8] Cheng, H., Wu, J., Yu, Q., Kim-Lee, H.-J., Carlson, A., Turner, K. T., Hwang, K.-C., Huang, Y., and Rogers, J. A., 2012, "An Analytical Model for Shear-Enhanced Adhesiveless Transfer Printing," Mechanics Research Communications, 43(pp. 46-49.

[9] Kim, T. H., Carlson, A., Ahn, J. H., Won, S. M., Wang, S. D., Huang, Y. G., and Rogers, J. A., 2009, "Kinetically Controlled, Adhesiveless Transfer Printing Using Microstructured Stamps," Applied Physics Letters, 94(11), pp. 113502.

[10] Childs, W. R., and Nuzzo, R. G., 2002, "Decal Transfer Microlithography: A New Soft-Lithographic Patterning Method," Journal of the American Chemical Society, 124(45), pp. 13583-13596.

[11] Childs, W. R., and Nuzzo, R. G., 2004, "Patterning of Thin-Film Microstructures on Non-Planar Substrate Surfaces Using Decal Transfer Lithography," Advanced Materials, 16(15), pp. 1323-1327.

[12] Childs, W. R., Motala, M. J., Lee, K. J., and Nuzzo, R. G., 2005, "Masterless Soft Lithography: Patterning Uv/Ozone-Induced Adhesion on Poly(Dimethylsiloxane) Surfaces," Langmuir, 21(22), pp. 10096-10105.

[13] Childs, W. R., and Nuzzo, R. G., 2005, "Large-Area Patterning of Coinage-Metal Thin Films Using Decal Transfer Lithography," Langmuir, 21(1), pp. 195-202.

[14] Hines, D. R., Mezhenny, S., Breban, M., Williams, E. D., Ballarotto, V. W., Esen, G., Southard, A., and Fuhrer, M. S., 2005, "Nanotransfer Printing of Organic and Carbon Nanotube Thin-Film Transistors on Plastic Substrates," Applied Physics Letters, 86(16), pp. 163101.

[15] Saeidpourazar, R., Li, R., Li, Y. H., Sangid, M. D., Lu, C. F., Huang, Y., Rogers, J. A., and Ferreira, P. M., 2012, "Laser-Driven Non-Contact Transfer Printing of Prefabricated Microstructures," Journal of Microelectromechanical Systems, (to appear)(pp.

[16] Li, R., Li, Y., Lü, C., Song, J., Saeidpourazar, R., Fang, B., Zhong, Y., Ferreira, P. M., Rogers, J. A., and Huang, Y., 2012, "Thermo-Mechanical Modeling of Laser-Driven Non-Contact Transfer Printing: Two-Dimensional Analysis," Soft Matter, 8(pp. 3122-3127.

[17] Suh, D., Choi, S. J., and Lee, H. H., 2005, "Rigiflex Lithography for Nanostructure Transfer," Advanced Materials, 17(12), pp. 1554-1560.

[18] Yang, W., Yang, H., Qin, G., Ma, Z., Berggren, J., Hammar, M., Soref, R., and Zhou, W., 2010, "Large-Area Inp-Based Crystalline Nanomembrane Flexible Photodetectors," Applied Physics Letters, 96(12), pp. 121107.

[19] Varenberg, M., and Gorb, S., 2007, "Shearing of Fibrillar Adhesive Microstructure: Friction and Shear-Related Change in Pull-Off Force," J. R. Soc. Interfaces, 4(pp. 721.

[20] Aksak, B., Murphy, M. P., and Sitti, M., 2008

[21] Jeong, H. E., Lee, J.-K., Kim, H. N., Moon, S. H., and Suh, K. Y., 2009, "A Nontransferring Dry Adhesive with Hierarchical Polymer Nanohairs," Proceedings of the National Academy of Sciences of the United States of America, 106(14), pp. 5639-5644.

[22] Murphy, M., Aksak, B., and Sitti, M., 2009, "Gecko Inspired Directional and Controllable Adhesion," Small, 5(pp. 170.

[23] Kramer, R. K., Majidi, C., and Wood, R. J., 2010, "Shear-Mode Contact Splitting for a Microtextured Elastomer Film," Adv. Mater., 22(pp. 3700.

[24] Carlson, A., Wang, S., Elvikis, P., Ferreira, P. M., Huang, Y., and Rogers, J. A., 2012, "Active, Programmable Elastomeric Surfaces with Tunable Adhesion for Deterministic Assembly by Transfer Printing," Advanced Functional Materials, pp.

[25] Nguyen, T. D., Govindjee, S., Klein, P. A., and Gao, H., 2004, "A Rate-Dependent Cohesive Continuum Model for the Study of Crack Dynamics," Computer Methods in Applied Mechanics and Engineering, 193(30-32), pp. 3239-3265.

[26] Nguyen, T. D., Govindjee, S., Klein, P. A., and Gao, H., 2005, "A Material Force Method for Inelastic Fracture Mechanics," Journal of the Mechanics and Physics of Solids, 53(1), pp. 91-121.

[27] Schapery, R. A., 1975, "A Theory of Crack Initiation and Growth in Viscoelastic Media. I. Theoretical Development " International Journal of Fracture, 11(1), pp. 141-159.

[28] Schapery, R. A., 1975, "A Theory of Crack Initiation and Growth in Viscoelastic Media. Ii. Approximate Methods of Analysis," International Journal of Fracture, 11(3), pp. 369-388.

[29] Gent, A. N., and Petrich, R. P., 1969, "Adhesion of Viscoelastic Materials to Rigid Substrates," Proceedings of the Royal Society of London Series a-Mathematical and Physical Sciences, 310(1502), pp. 433-448.

[30] Hui, C.-Y., Xu, D.-B., and Kramer, E. J., 1992, "A Fracture Model for a Weak Interface in a Viscoelastic Material (Small Scale Yielding Analysis)," Journal of Applied Physics, 72(8), pp. 3294.

[31] Nguyen, T. D., and Govindjee, S., 2006, "Numerical Study of Geometric Constraint and Cohesive Parameters in Steady-State Viscoelastic Crack Growth," International Journal of Fracture, 141(1-2), pp. 255-268.

[32] Rahulkumar, P., Jagota, A., Bennison, S. J., and Saigal, S., 2000, "Cohesive Element Modeling of Viscoelastic Fracture: Application to Peel Testing of Polymers," International Journal of Solids and Structures, 37(13), pp. 1873-1897.

[33] Slanik, M. L., Nemes, J. A., Potvin, M. J., and Piedboeuf, J. C., 2000, "Time Domain Finite Element Simulations of Damped Multilayered Beams Using a Prony Series Representation," Mechanics of Time-Dependent Materials, 4(3), pp. 211-230.

[34] Tada, H., Paris, P. C., and Irwin, G. R., 2000, *The Stress Analysis of Cracks Handbook* American Society of Mechanical Engineers, New York.

[35] Huang, Y. G. Y., Zhou, W. X., Hsia, K. J., Menard, E., Park, J. U., Rogers, J. A., and Alleyne, A. G., 2005, "Stamp Collapse in Soft Lithography," Langmuir, 21(17), pp. 8058-8068.

[36] Abaqus Analysis User's Manual V6.9 (Dassault Systemes, Pawtucket, Ri, 2009)

[37] Chaudhury, M. K., and Whitesides, G. M., 1991, "Direct Measurement of Interfacial Interactions between Semispherical Lenses and Flat Sheets of Poly(Dimethylsiloxane) and Their Chemical Derivatives," Langmuir, 7(5), pp. 1013-1025.

Figure Captions

Figure 1. An illustration of stamp/ink system (left) and the stamp geometry consisting of a post and a backing layer (right).

Figure 2. The storage modulus of PDMS versus the frequency at room temperature. The theory is based on a 2nd order Prony series (N=2) with Young's modulus $E_\infty = 1.32\,\text{MPa}$, and parameters in the Prony series g_1=0.102, g_2=0.209, τ_1=0.426 s and τ_2=0.0167 s.

Figure 3. The crack tip energy release rate versus time for the crack length a = 2.5 μm, post width L = 100 μm, and applied stress rate $\dot{\sigma} = 5.86\times10^5$ Pa/s.

Figure 4. The normalized critical time t_c/τ_1 versus the non-dimensional combination of applied stress rate, crack length, Young's modulus and interfacial toughness $\left(\dot{\sigma}\tau_1\right)^2 a/\left(E_\infty \Gamma_0\right)$.

Figure 5. The pull-off force to delaminate a PDMS stamp from a silicon ink versus the pulling speed.

Journal of Applied Mechanics. Received August 04, 2012;
Accepted manuscript posted October 23, 2012. doi:10.1115/1.4007851

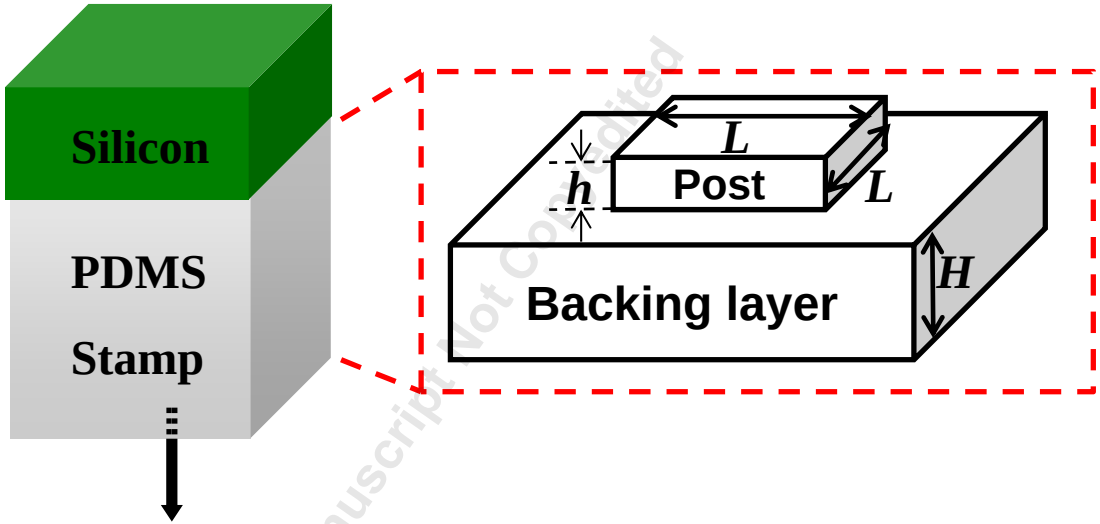

Figure 1

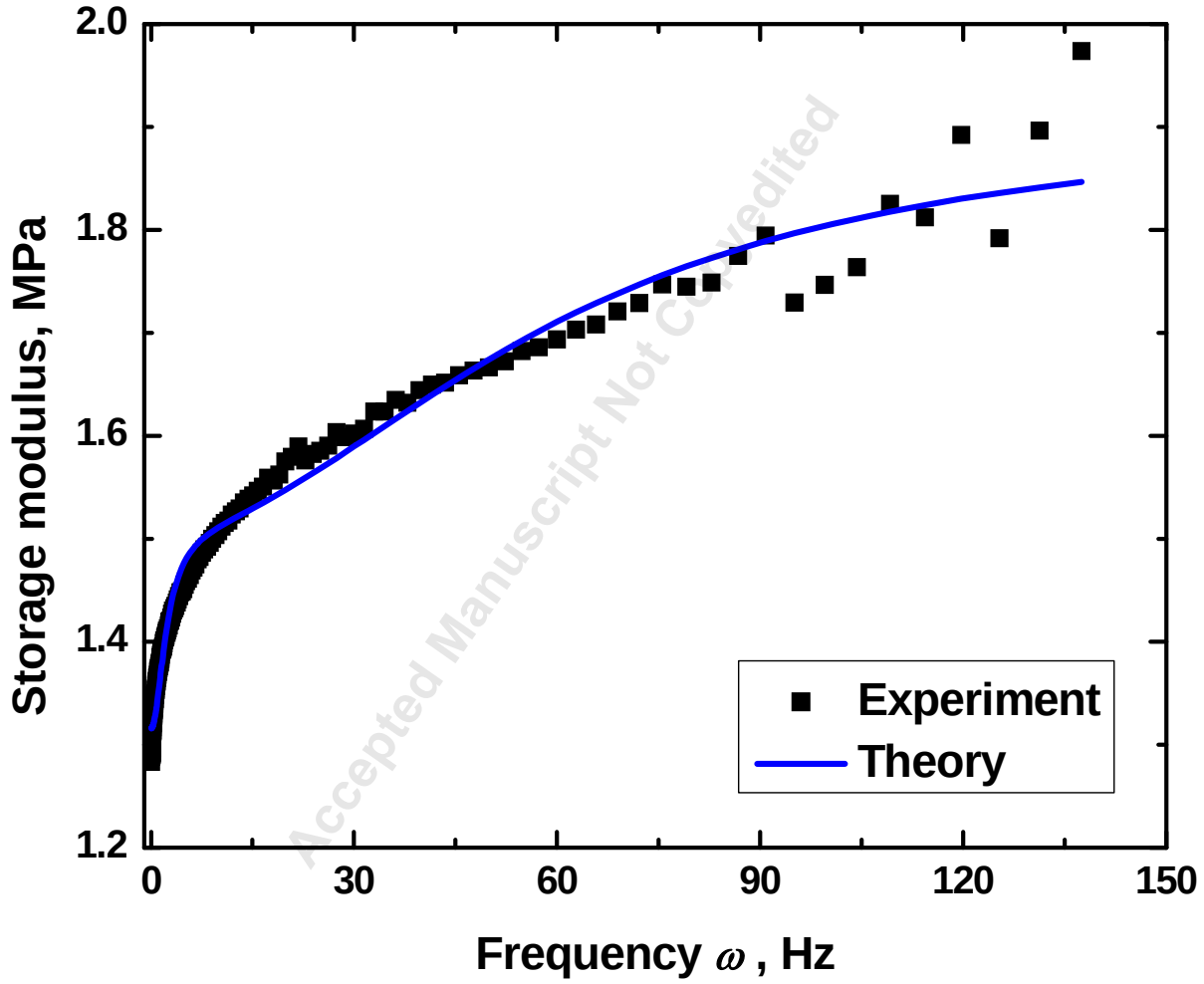

Figure 2

Journal of Applied Mechanics. Received August 04, 2012;
Accepted manuscript posted October 23, 2012. doi:10.1115/1.4007851

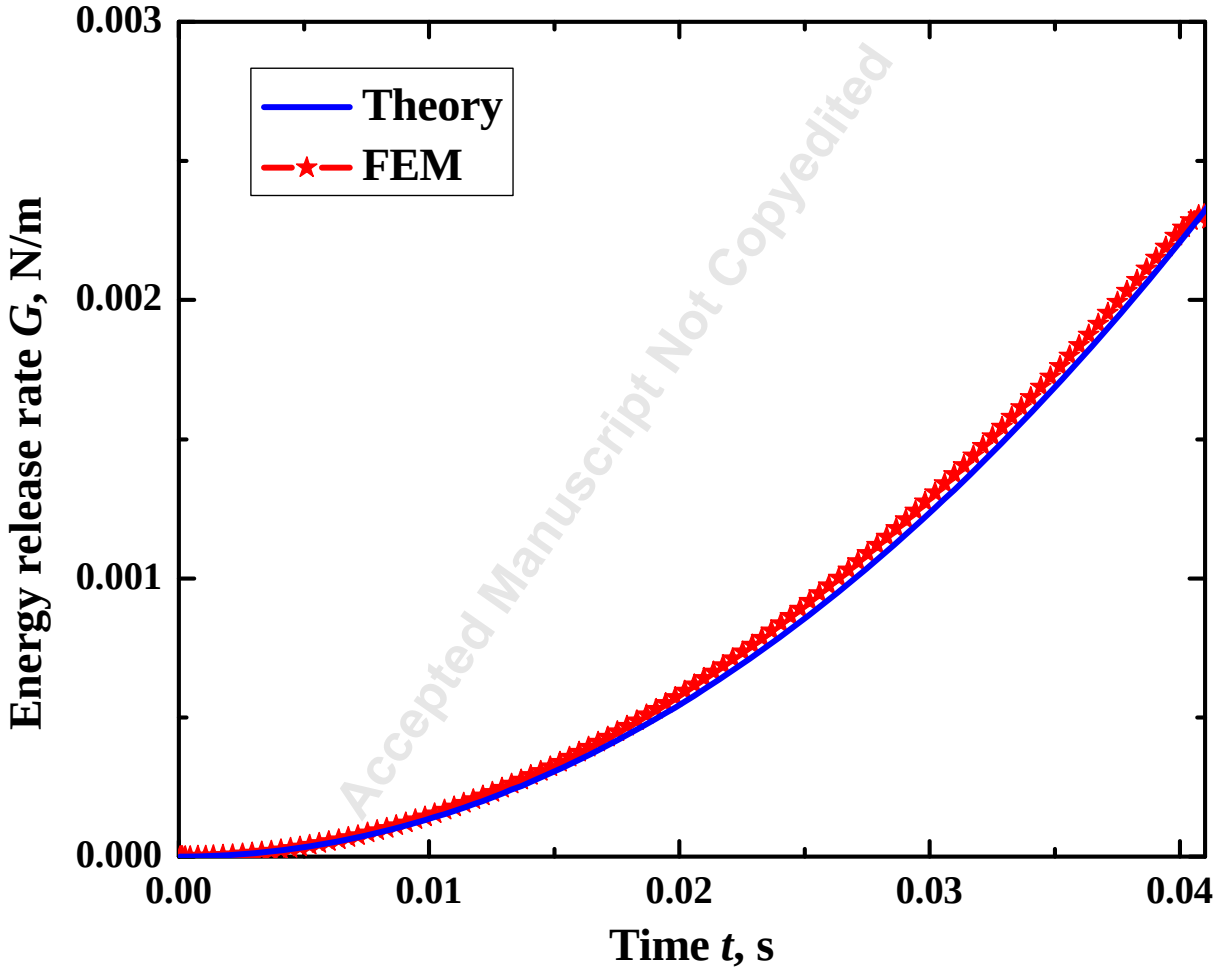

Figure 3

Journal of Applied Mechanics. Received August 04, 2012;
Accepted manuscript posted October 23, 2012. doi:10.1115/1.4007851

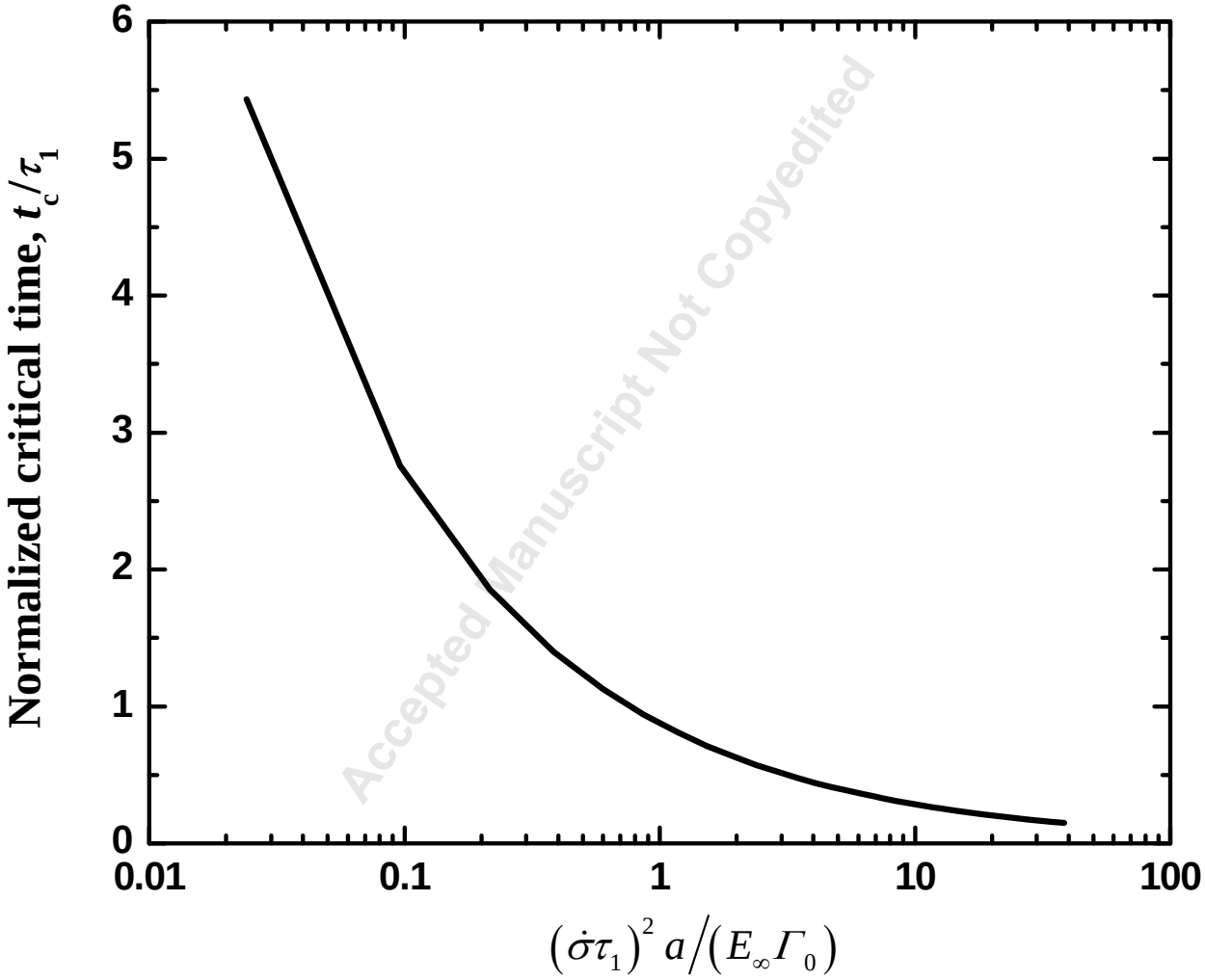

Figure 4

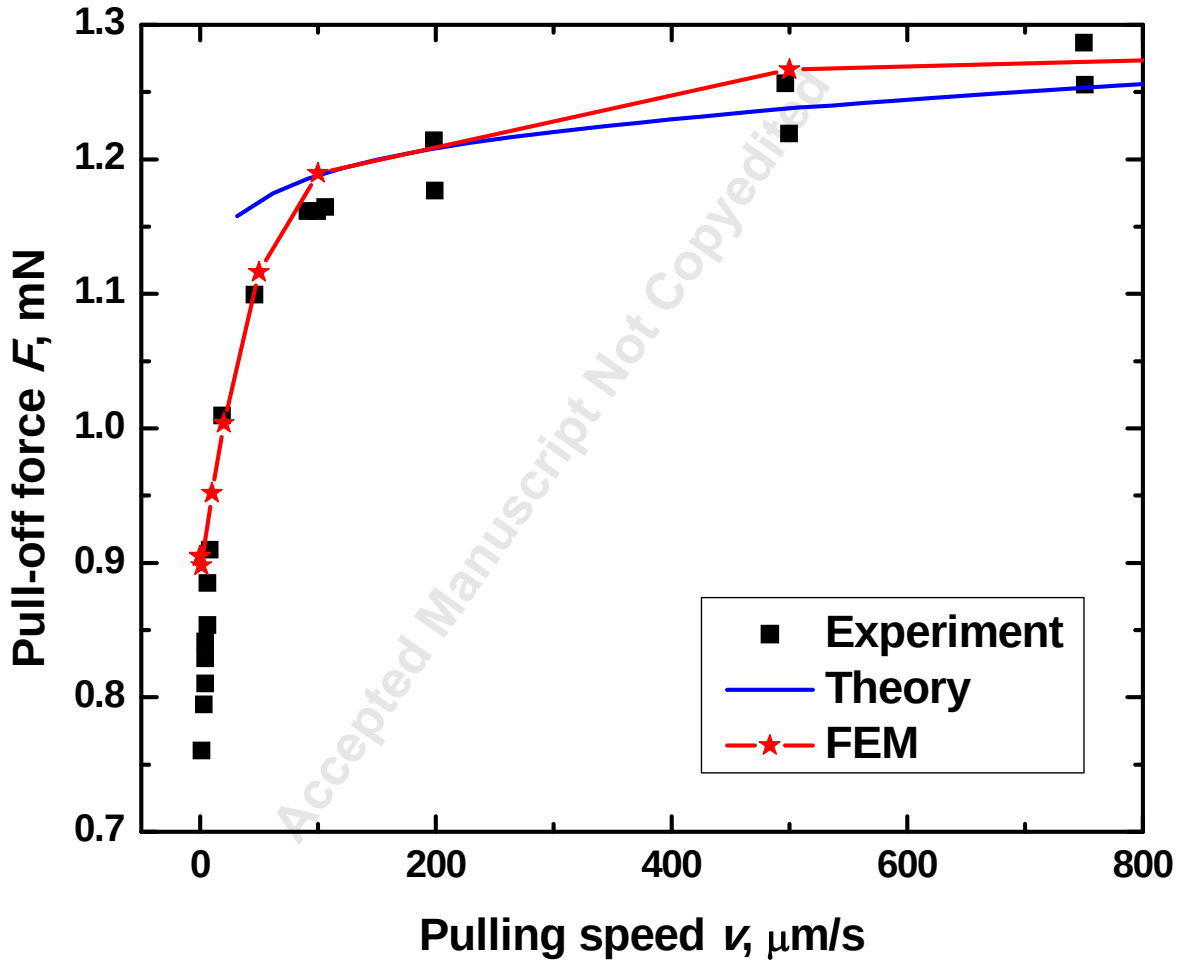

Figure 5